Toric offset three-reflector antenna for an advanced microwave limb sounder

Richard E. Cofield, Thomas A. Cwik, Nasrat A. Raouf

Jet Propulsion Laboratory, 4800 Oak Grove Drive, Pasadena, CA 91109-8099, USA

ABSTRACT

An advanced Microwave Limb Sounder (MLS), now in concept development for a potential future mission, is a space-borne heterodyne instrument to measure pressure, temperature, and atmospheric constituents from thermal emission between 120 and 2400 GHz. Previous MLS instruments used pencil-beam antennas sized to resolve ~ 1 vertical scale height. Current atmospheric models need better horizontal resolution than orbit spacing provides. To meet these needs, a new antenna concept combines the wide scan range of the parabolic torus with unblocked offset Cassegrain optics. The resulting system is diffraction-limited in the vertical plane but extremely astigmatic, with beamwidths $0.13\times2.5°$. Nadir axis symmetry ensures that this Beam Aspect Ratio (BAR) is invariant over $\pm33°$ of azimuth. The antenna can feed either an array of receivers or multiplexed low-noise receivers whose FOVs are swept by a small scanning mirror. We describe 3 stages of antenna design: First, using a paraxial-optics method, we choose conic profiles given vertical resolution orbit geometry, then develop the surfaces by nadir axis rotation, matching axisymmetric feeds to the BAR. A ray-trace program validates the design and generates alignment and deformation tolerances. Finally, a physical optics analysis verifies reflector surface currents and radiation patterns.

Keywords: microwave limb sounding, wide FOV, toroidal reflectors, Gaussian beams, physical optics

1. INTRODUCTION

Microwave limb sounding is a technique[1] which provides atmospheric measurements by sensing thermal emission in millimeter-wavelength spectral bands with heterodyne radiometers. Previous Microwave Limb Sounder (MLS) instruments include one launched on board NASA's Upper Atmosphere Research Satellite (UARS) in September 1991, and its successor EOS MLS, scheduled for launch on the Earth Observing System (EOS) Aura mission in 2004. Primary measurement suites have grown from the UARS set of stratospheric profiles of ClO, O_3, H_2O, temperature, and field-of-view (FOV) tangent point pressure which provides the pointing reference and vertical coordinate for the other geophysical quantities. Additional products targeted by EOS MLS include geopotential height, HCl, HNO_3, OH, upper tropospheric H_2O, and many other species which have low abundances but are nonetheless detectable with the limb sounding geometry.

In order to maximize vertical resolution yet take advantage (within spacecraft envelope constraints) of the weak horizontal dependence of limb radiance, the previous MLS instruments have optics which couple pencil beams, with a 2:1 Beam Aspect Ratio (BAR), to circularly symmetric feed horns. Perforated plates (used as low-pass dichroic filters) and wire grid polarizers multiplex the beams to radiometer front ends at frequencies from 63 to 660 GHz. To maximize the time observing Earth's limb, the radiometers are operated in total power mode. Hence for radiometric calibration, in which we periodically switch radiometers to view ambient blackbody targets and cold space, the optics must provide beam waists (or moderately small parts of the signal path) which accommodate switching or chopping mirrors.

Future missions need better horizontal resolution than the single measurement track of the previous MLS instruments. Ideally, FOV smearing in the horizontal from spacecraft motion (7.7km/s) during a vertical scan

Further author information: (Send correspondence to R.E.Cofield)
R.E.Cofield: E-mail: Richard.E.Cofield@jpl.nasa.gov, Telephone: (818) 354-2501, Fax: (818) 393-5065
T.A.Cwik: E-mail: Thomas.A.Cwik@jpl.nasa.gov, Telephone: (818) 354-4386
N.A.Raouf: E-mail: Nasrat.A.Raouf@jpl.nasa.gov, Telephone: (818) 354-0085

should be similar to the azimuth spacing of the beams. Radiative transfer limits line-of-sight resolution to $\sim$ 100 km, compared to orbit spacing $\sim$ 2500 km. Current receiver technology allows for reduced integration times or arraying to achieve 25$\times$ more coverage in azimuth (cross-track direction), so that an antenna is needed with a BAR of the same order (25:1).

The robust scan range of the spherical reflector has been familiar to radio astronomers since the construction of the Arecibo radio telescope. A rotating radiometer/feed antenna, developed some years ago for a space shuttle-based microwave imaging application,[2] proposed an offset fed parabolic torus for unblocked nadir cross-track scanning ($\pm 60°$) between 0.6 and 120 GHz, and verified the low frequency performance using scale model measurements. The Array MLS (AMLS) antenna is an outgrowth of these designs, adapted for conical limb scanning of the atmosphere, with the offset dual reflector configuration providing zero blockage. The antenna couples a "pancake" beam incident from the limb to an array of mixer feed horns having circular beamwidths of order 15°, typically used for passive microwave radiometry at these frequencies.

2. REQUIREMENTS

The AMLS is designed for a polar sun-synchronous nearly circular orbit. From a platform altitude between 700 and 900 km, the limb is between 3000 and 3400 km distant. For the 700 km orbit, an instantaneous footprint volume of $5.3 \times 120 \times 150$ km (elevation $\times$ azimuth $\times$ axial) corresponds to a Half Power Beam Width (HPBW) of $0.13 \times 2.5°$. A spacing of 2500 km between consecutive tangent tracks at the equator means 20 FOVs overlap at about the -3 dB points in azimuth. The azimuth scan range is extended to $\pm 33°$ to cover the poles and to overlap coverage with that of the previous orbit.

The instrument's FOV must be scanned vertically over a 2° range with a period of about 26 seconds, to cover limb tangent heights from 0 to $\sim$ 100 km in the given orbit. We augment this range by 0.5° for Earth oblateness over the course of an orbit, another 0.5° for mounting uncertainty and attitude control, and additional $[-4, +5]°$ for occasional (monthly or yearly) scans high above the atmosphere to calibrate the spectral variation of sidelobes far from the main beam. The net vertical scan range required is $\pm 6°$.

Since the limb radiance varies extremely rapidly with nadir angle over this range (equivalent black body temperatures from 2.7 up to 300 Kelvin), the retrieval algorithms are quite sensitive to both errors and variation with scan of the measured FOV function. This, plus the time required to measure FOV functions in pre-launch calibration, has precluded the use of sub-reflector scanning or feed arraying in previous MLS instruments. For example, the scan range required is $\sim 70 \times$HPBW, whereas the small f/D antennas which can be accommodated on typical launch vehicles have focal plane scanning of only $\sim 12\times$ HPBW before FOV degradation becomes unacceptable. Therefore, the AMLS design has anticipated only a few pixels' worth of vertical arraying, relying instead on the same mechanical scan of the entire antenna which has been used in previous missions.

The rapid growth of radiance with limb tangent height also means that the boresight direction of the FOV function must be known to a few tens of arc seconds. Previous MLS instruments have used the Moon as a calibration source for refining pointing estimates obtained in pre-launch calibration.[3] The Moon will not fill the elongated FOV of AMLS, so this method will lose some sensitivity. Finally, a key parameter for observing extended atmospheric sources is the *beam efficiency*, defined as the fractional power enclosed in the FOV within $2.5 \times$HPBW (the historical factor 2.5 is the location of the 1st null of the Fraunhofer pattern of a moderately apodized circular aperture). Beam efficiency of the AMLS FOV must exceed 90% and be known within 1%.

2.1. Feed Requirements

The AMLS design described here was planned for an array of receivers based on Millimeter-wave Monolithic Integrated Circuit (MMIC) detectors. These have footprints of the order of the beam waist size and low enough power consumption to be arrayed; the pixel size is about 1×1 inch. The feed surface of such an array must be concave, allowing access to IF cables and tuning hardware at the back ends. We have also studied detectors based on Superconductor-Insulator-Superconductor (SIS) junction and Hot Electron Bolometer (HEB) technologies. These have such low receiver noise figures that azimuth measurements can be time-shared, using a small scanning mirror to sweep FOVs of single pixels (multiplexed for the frequency ranges as in UARS and EOS MLS) over the AMLS antenna. For this Scanning MLS (SMLS) concept, we replace the requirement of a

concave feed surface by a requirement to produce a small beam on the scanning mirror. As discussed below, this relaxes some constraints on the paraxial design, and will be the subject of our future work.

3. DESIGN AND ANALYSIS

3.1. Paraxial Design

Given orbit geometry and the beamwidth requirements on the antenna, we choose a conventional dual-offset Cassegrain for reflector profiles in the vertical plane. A dual reflector configuration is required to get both long effective focal length for the feed horn and the compact antenna for the launch vehicle envelope. We prefer the Cassegrain over the Gregorian to minimize the envelope of the antenna in the direction of flight; in fact, the tops of both primary and secondary reflector have the same z position along the direction of Earth's limb. An apodization of -15 dB on the primary's edge and a projected aperture height of 1.6 m give a reasonable balance between spillover, beam efficiency and vertical resolution. We do not shape the vertical profiles away from conic sections. The parent parabola has 1 m focal length, resulting in a parent $f/D = 0.25$ which can be manufactured with surface figure tolerances in the 5–15 μm range.

The conventional parabolic torus configuration, with $R_0 = 2f$, was found to be too big ($\geq$ 2 m) and poorly arrayed, with feeds separated by 0.2m on the feed arc. A cylindrical antenna (toric axis at infinity), though attractive by its low fabrication cost, is likewise too large.

Thus, given a set of reflector profiles and a toric axis inclined to the optic axis according to the orbit geometry, we vary the position of the toric axis until a circularly symmetric feed is matched to the desired far field BAR. This design step must result in physically realizable reflector outlines (the toric axis must not pass through a reflector) and satisfy feed constraints described above. The latter constraints, especially that the feed surface be concave, combine with the need for a volume where all beams are confined to fit on a calibration switching mirror. These force us from 2 to 3 curved mirrors. Moreover, both the secondary and tertiary reflectors are saddle-shaped. To remedy this for the secondary would require making the configuration Gregorian. We will also reexamine the tertiary, for the SMLS case of single-pixel cooled receivers. We will keep the requirement to confine the beam, however, whether as a switching mirror for the MMIC array or as switching and scanning mirrors for the single pixel.

Figure 1 is the design curve for the three-reflector antenna. The ordinate is the sagittal magnification $\mathcal{M}_{\text{sag}}$, defined as the ratio of the angle of a paraxial pencil of rays incident on the antenna from Earth's limb to the angle of the same pencil incident on the focal surface. A spreadsheet calculates $\mathcal{M}_{\text{sag}}$ from the principal radii of curvature and ray incidence angles at the chief ray points on each surface, *i.e.* by paraxial Gaussian ray tracing. As the toric axis is moved along the z axis, the sagittal radii of curvature of the reflectors change and $\mathcal{M}_{\text{sag}}$ varies accordingly. The case $z_{TP} = \pm\infty$ corresponds to conic cylindrical surfaces, swept out by translating the profiles normal to the vertical plane. Since the reflectors have no sagittal curvature for this case, the horizontal asymptote is $\mathcal{M}_{\text{sag}} = +1$.

The three poles of the function $\mathcal{M}_{\text{sag}}(z_{TP})$ correspond to the toric axis passing through a reflector. These physically unrealizable regions are marked in the figure. The pair of horizontal lines just above and below the z_{TP} axis are the values of $\mathcal{M}_{\text{sag}}$ which give the desired horizontal beamwidth. One line corresponds to converging sagittal rays entering the antenna, the other to diverging rays, i.e. a sagittal focus between the scene and primary reflector. The design choice between these two lines is of little consequence, since the aperture size is dominated by the diffraction-limiting vertical extent of the aperture, rather than whether the sagittal focus is real (in front of the primary) or virtual (behind it). We therefore let reflector size (in this case, the tertiary's) and feed spacing dictate which line is chosen for the solution. In Figure 1 the distance from the z_{TP} axis to either line is a function of the horn beamwidth, which was determined by the elevation plane design. Thus any intersection point of either horizontal line with the curve $\mathcal{M}_{\text{sag}}(z_{TP})$ is a candidate design which meets the far-field beamwidth requirement. Although axisymmetric horns are easier to fabricate in the sub-millimeter wavelength range, a cleaner layout for the case presented here results from a horn BAR of 0.8:1, which is readily achieved for frequencies below 300 GHz. We expect to revisit the issue of feed symmetry as the design and horn technology mature.

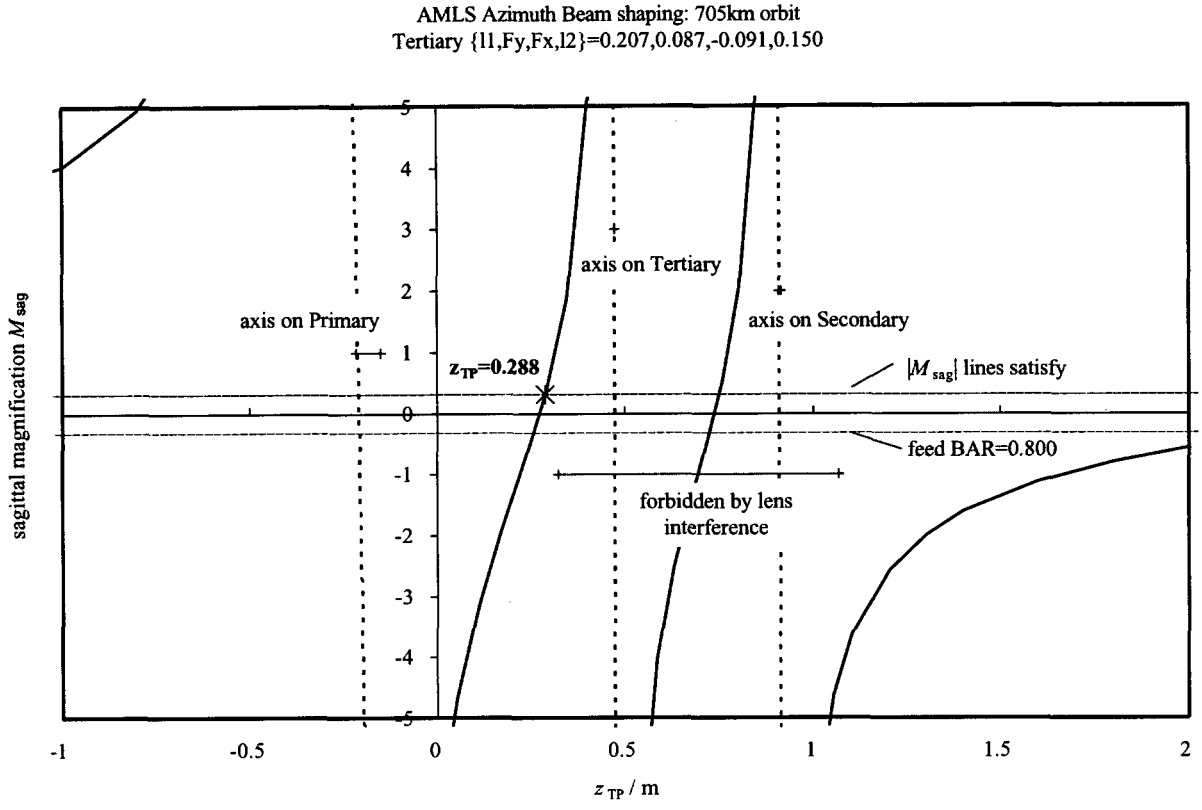

Figure 1. Sagittal Magnification vs. toric axis position, from AMLS paraxial design.

Another segment of the z_{TP} domain is forbidden by the finite size of the pixel apertures, again determined by the elevation plane design. These constraints, plus looser constraints on the size of the antenna envelope allowed by the launch vehicle, restrict the solutions to the pair for which the toric axis runs between the primary and tertiary reflectors. Of these two the value $z_{TP} = 0.288$ minimizes the size of the tertiary and secondary.

The final step in this paraxial analysis was propagation of a zeroth-order Gaussian beam back from the feed horn to the primary aperture. This has been an important step in the two previous MLS instruments, where signal wavelengths are large enough that the secondary and subsequent reflectors are in the intermediate field of the signal beam waist, and Gaussian beam optics are required to position and size optical elements.[4] A section of the design spreadsheet performs the Gaussian mode propagation and provides the extent of the forbidden regions in Figure 1. In Gaussian propagation the transition between near and far field occurs at the Rayleigh distance $z_R = \pi\ w_0^2/\lambda$, where w_0 is the distance from the optic axis to a radius where the electric field has $1/e$ of its magnitude on axis. The smallest value of sagittal z/z_R is 4.2 on the tertiary reflector, which indicates that the reflector outlines based on geometrical optics are good starting points for the subsequent analyses, and that the axial beam waist displacement will be a small perturbation to the layout.

3.2. Design Verification

The antenna system was modeled in code V®, a proprietary optical analysis program developed by Optical Research Associates of Pasadena, California. The principal applications of this software to the previous MLS designs have been to verify Gaussian beam propagation predictions of the paraxial model, and to develop alignment and thermal deformation sensitivities using the powerful tolerancing capabilities of Code V.

A large parabolic cylinder, with focal line passing through the outer sagittal focus, was defined in front of the primary. This simulates radiation incident from Earth's limb and defines the aperture. For the toric reflectors,

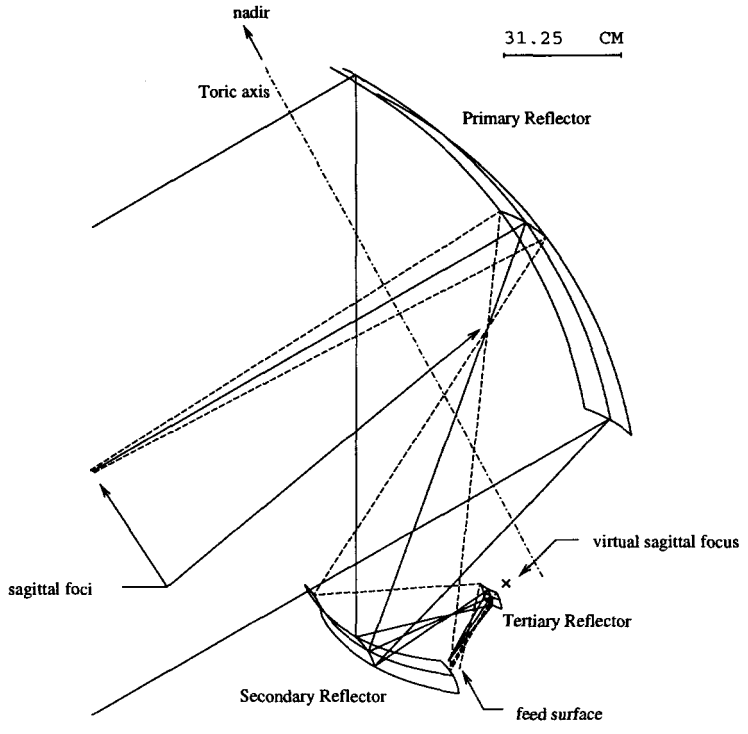

Figure 2. Ray trace through the AMLS antenna for a single pixel, showing chief and edge rays, aperture projections and the toric axis.

user-defined subroutines were developed to calculate $z(x, y)$ given coordinates x and z in the chief ray tangent plane of each reflector. Ray tracing also requires the local surface normal, expressed as partial derivatives $\partial z/\partial x$ and $\partial z/\partial y$. Code V offers to calculate these by a finite difference method, but software had been developed previously for least-squares fitting of a perturbed conic toric to coordinate measurement machine (CMM) data.[5] This software calculated the gradient $\nabla f(x, y, z)$ of the toric surface $f(x, y, z) = 0$, and has since been adapted to the Code V subroutine; this speeds the calculation of large numbers of rays needed for surface optimization, alignment and thermal deformation studies, and scalar diffraction calculations in Code V.

Figure 2 is a view of the antenna as modeled by Code V, showing apertures projected onto the reflectors, the chief and edge rays, and the toric axis. The sagittal foci and reflector outlines match the predictions of the paraxial design model.

3.2.1. Results of geometrical ray tracing

Spot diagrams were generated at several planes along the optical path, and the corresponding footprint plots were compared with the surface current maps from the physical optics mode described below. These confirmed the assertion of the paraxial design that all reflectors are well separated from any caustic surfaces. The lens reversal feature of Code V was applied to the entire optical system, which was then fed by a bundle of rays at the nominal feed location. Reflector intersections of the chief and edge rays matched those for the forward propagation, to within the allowable margin for reflector outlines. Spot diagrams at aperture and feed surfaces showed the

expected reciprocity between forward and reversed systems. Point spread functions were not calculated, as the diffraction analysis tools provide better insight due to the large edge tapers (apodizations).

Comparison of the Optical Path Difference (OPD) maps for different field angles confirmed the limitation of vertical arraying to about 5 pixels before the wavefront error (and therefore the elevation pattern) degrades severely. This validates our decision to retain the mechanical option of previous MLS instruments for the $\pm 6°$ of limb vertical scanning.

3.2.2. Scalar diffraction analyses

Code V's Gaussian beam analysis confirmed the propagation of the fundamental Gaussian mode through the antenna. For the EOS MLS program, a user-defined routine had been written to calculate the Gaussian beam overlap integral, a function of the nominal and perturbed beam waist size, position, decenters and tilts. This Strehl ratio provided an alternative cost function to Code V's tolerance engine, and had been used to derive alignment sensitivities, set optical element position tolerances, and calculate correction shims during receiver alignment of the EOS MLS radiometers. Repeating this analysis for the AMLS antenna resulted in an alignment sensitivity matrix similar to that of EOS MLS; typical placement tolerances for the AMLS reflectors are ± 0.001 inch and $0.03°$.

A scalar diffraction option was added to Code V some months after the Gaussian propagation was analyzed. Although we have not yet applied the new analysis tool to the AMLS antenna, we used it to confirm the amplitude and phase beam patterns measured for the EOS MLS feed mirrors during design and testing. It predicts the far sidelobe shape and phase centers of these 2:1 BAR astigmatic beams, in good agreement with the measured patterns, and confirms the need to keep conic sections in the tangential plane to avoid beam shape distortion. We plan to apply this tool to the AMLS antenna when we repeat tolerance studies for future design iterations.

3.3. Implementation

Figure 3 is a mechanical layout of the antenna, using reflector surfaces swept out from the Code V outlines by $\pm 33°$, to accommodate the azimuth scan desired in orbit. The instrument comprises the antenna, support structure, and a radiometer chassis in which the beams from the tertiary are separated by frequency and polarization for coupling to the receivers. It will be mounted on the nadir side of the spacecraft. Not shown are: (1) the calibration switching mirror which diverts the receiver views to cold space and to blackbody targets, (2) the scanning mirror which would select different parts of the antenna for scanning by a single receiver, (3) the elevation scanning mechanism, (4) a spectrometer assembly which processes down-converted signals from the receivers, and (5) radiator surfaces which shed the heat from receiver electronics and from cryocoolers in the case of the single cooled receiver. We are currently studying deployment schemes, such as rotating the primary about an axis near its support attachment to a launch/stow position along the direction which becomes the orbital velocity vector.

Table 1 summarizes reflector dimensions for the antenna. Despite the saddle shape of the secondary and tertiary, and the elongation of the secondary, the alignment and surface figure tolerances are loose enough at the signal frequencies to make us confident that the experience in manufacturing UARS and EOS MLS reflector antennas will make the AMLS antenna achievable as well.

3.4. Physical Optics

A physical optics model of the three-reflector system was developed using the integrated design environment MODTool. The model calculates the far-field radiation pattern from a reflector system illuminated by a given feed pattern: surface currents excited on the tertiary reflector are integrated to calculate illumination on the secondary. Its surface currents are then integrated to illuminate in turn the primary reflector, and so on to the far field. By the Lorentz reciprocity theorem, this far-field pattern is the conjugate match to the single mode represented by the feed horn pattern when the antenna acts as a receiver. We swept out reflector surfaces from the generating profiles by $\pm 50°$, somewhat larger than in Figure 3, so that surface currents could be evaluated in the regions which become spillover when reflectors are trimmed to their final size.

Table 1. AMLS Reflector shapes and dimensions.

primary reflector	
Shape	Tilted Parabolic Torus
Parent f	1 m
Parent f/D	0.25
Dimensions	1.9×0.7 m
	for 1.6 m projected vertical aperture
Radii of Curvature (ROC)	$-0.41 \times [-2.1, -5.7]$ m (sagittal×tangential)
secondary reflector	
Shape	Tilted Hyperbolic Torus
Dimensions	0.40×1.10 m
chief ray point ROC	$+0.2 \times -0.56$ m
tertiary reflector	
Shape	Tilted Elliptical Torus
Dimensions	0.20×0.30 m
chief ray point ROC	$-0.18 \times +0.19$ m

The physical optics model provides further verification of the design, including vector diffraction. It provides superior treatment of cross-polarization effects which become significant for highly curved reflectors such as the tertiary and secondary. Finally, the superposition of direct and scatted patterns permits a straightforward and rigorous evaluation of spillover radiation, which in previous radiometer antenna systems has been shown to contribute significantly to systematic radiance offsets.[5] With the computing power and flexibility of the MODTool design environment (which combines thermal, structural and optic models on the same platform and software) a few degrees of freedom can readily be perturbed, *e.g.* to verify alignment and thermal or gravitational deformation sensitivities generated and optimized using the simpler optics models.

3.4.1. Model description

Feed pattern beamwidths are taken from the paraxial design or from the Gaussian mode initial condition. In this calculation the feed is linearly polarized in the x direction. The pattern is $\cos^q(\theta)$ in both E and H planes. Using $q = 225$ produces a 29.55 dB gain horn pattern with HPBW=6.4°.

Direct mathematical relations for the surface descriptions are not easily found. The physical optics diffraction software requires the surface definition $z(x, y)$ in a child coordinate system rotated and translated from the master system. Because of the unusual surface definition described by a rotation about the toric axis (where the toric axis is not coincident with an axis of the parent coordinate system) a spline fit to the surfaces was used. The spline definitions are those of the wide class Non-Uniform Rational B-Splines (NURBS). A library was used to create the spline fit to the three mirror surfaces to a very high degree of accuracy (less than $\lambda/1000$ rms). The use of the spline library is unique and sped the calculation of the prototype design relative to any other finite-difference methods.

Nevertheless, the calculation of ∇f in the child coordinate system, as described for the Code V model in Section 3.2, is useful for the perturbation and optimizations we anticipate as the design progresses. Accordingly, we adapted the calculation and coordinate transformation of the surface gradient to a rudimentary physical optics scattering code which requires the spherical polar quantities $R(\theta, \phi)$, $\partial R/\partial\theta$ and $\partial R/\partial\phi$. These are obtained after transforming the Cartesian gradient components from the local coordinate system, containing the specular point and the conic focal points, to the specular point coordinate system, using

$$\partial R/\partial\theta = R(\theta,\phi)\frac{\nabla f \cdot \hat{a}_\theta}{\nabla f \cdot \hat{a}_R}; \quad \partial R/\partial\phi = R(\theta,\phi)\frac{\nabla f \cdot \hat{a}_\phi}{\nabla f \cdot \hat{a}_R}.$$

Since this scattering code has predicted FOV patterns in good agreement with measured 2:1 BAR feed patterns of the EOS MLS, we are now coding it for incorporation in the MODTool physical optics model of AMLS.

3.4.2. Surface currents

The currents on reflector surfaces are both useful diagnostics of the intermediate steps of the physical optics models and visual confirmation of the geometrical optics sizing of reflectors. Contour maps of their distribution within the surface outlines can also suggest optimizations to the shape or outline of reflectors.

Surface currents on the three reflectors are displayed in Figure 4. The transformation of the circularly symmetric beam, incident on the tertiary, to the elongated illumination of the primary, is evident. The edge tapers on tertiary, secondary and primary reflectors appear to be below -40dB, -15dB, and -10dB respectively. These levels confirm the reflector outlines chosen in the paraxial design and verified in the Code V model.

The -10 dB bright spots on either side of the secondary's main lobe merit further study, as does the bulge away from $x = 0$ in the $-y$ portion of the primary. It is fortunate that this is the portion of the reflector closest to its support and hence most amenable to expanding the outline, should that be necessary. The ripples seen also in this $-y$ portion probably result from edge diffraction by the other reflectors, and can be investigated by perturbing their outlines.

3.4.3. Predicted FOV patterns

Elevation and azimuth patterns have been predicted for the nominal design and are shown in Figure 5. The appearance of the first azimuthal sidelobe, at -25 dB and ~2–3 HPBWs away from the main lobe's peak, is consistent with the -10dB edge taper seen in the primary reflector current distribution. The elevation cut shows a large (-15 dB) sidelobe on one side of the main lobe, and other features characteristic of coma lobes in scanned conventional reflectors; however, such asymmetries have also been measured at the -18dB level on UARS MLS[5] and can be tolerated as long as their shape is known to the software which retrieves atmospheric profiles from limb radiances. The ripples on the side opposite the coma lobe are also artifacts of edge diffraction; since they are significant only below -50dB relative to the main lobe, we expect that, as for the UARS MLS, it will suffice to characterize only their envelope in processing flight data.

Table 1 summarizes principal plane beamwidths, directivity and beam efficiency for the antenna at 120 GHz. The predicted efficiency lies between measured values of 91% for UARS MLS and 95% for EOS MLS, and even with contributions from spillover and surface tolerance, expected to subtract 1–3%, will meet requirements.

Table 2. Beamwidth, Directivity and Beam Efficiency for principal planes at 120 GHz.

	HPBW /°	Pointing /°	Peak Directivity/dB	Beam Efficiency (@2.5×HPBW)
elevation	0.13	0.03	50.9	94.8%
azimuth	2.52	-		

4. FURTHER WORK

We shall refine the design for the multiplexed receiver concept now baselined for SMLS. This involves locating a confined beam volume for the scanning mirror, and revisiting whether the tertiary profile still needs to be concave, since the forbidden region in Figure 1 will shrink or vanish altogether. We can resume detailed design of the switching/chopping mirror when we know whether it is on the receiver or (worse) on the antenna side of the scanning mirror, and can then implement the space and calibration target views. If the launch vehicle can tolerate an enlarged instrument envelope, the system could be made a Gregorian, having a simpler secondary reflector. As the SMLS instrument concept matures we shall construct a breadboard antenna for pattern testing on one of the cylindrical Near Field Ranges at JPL.

Some work remains to update the mathematical models: the scalar diffraction (beam propagation) option of Code V will be run, and the surface gradient calculation will be ported to the MODTool physical optics model. We shall continue to evaluate surface currents, refine reflector outlines and shapes, and diagnose the irregular features of the surface current distributions and FOV patterns.

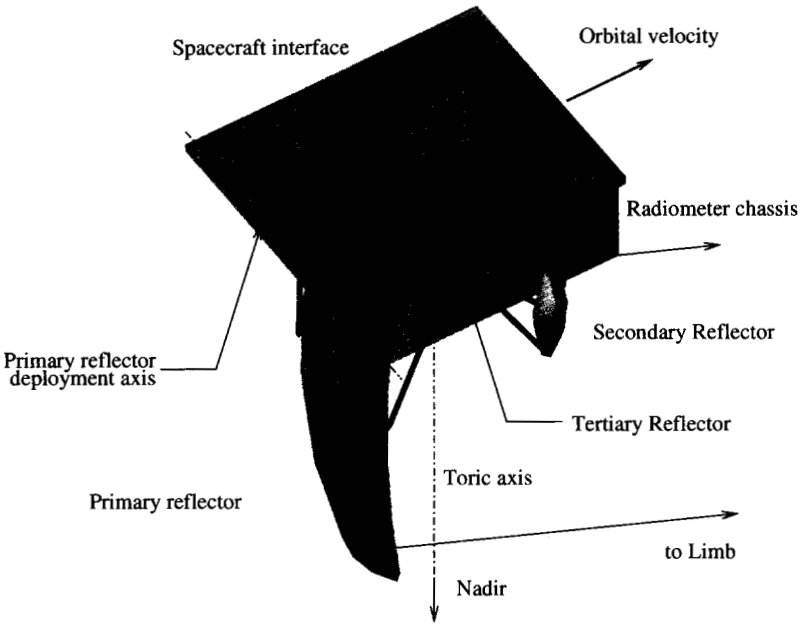

Figure 3. Layout of antenna and radiometer on spacecraft for the SMLS concept.

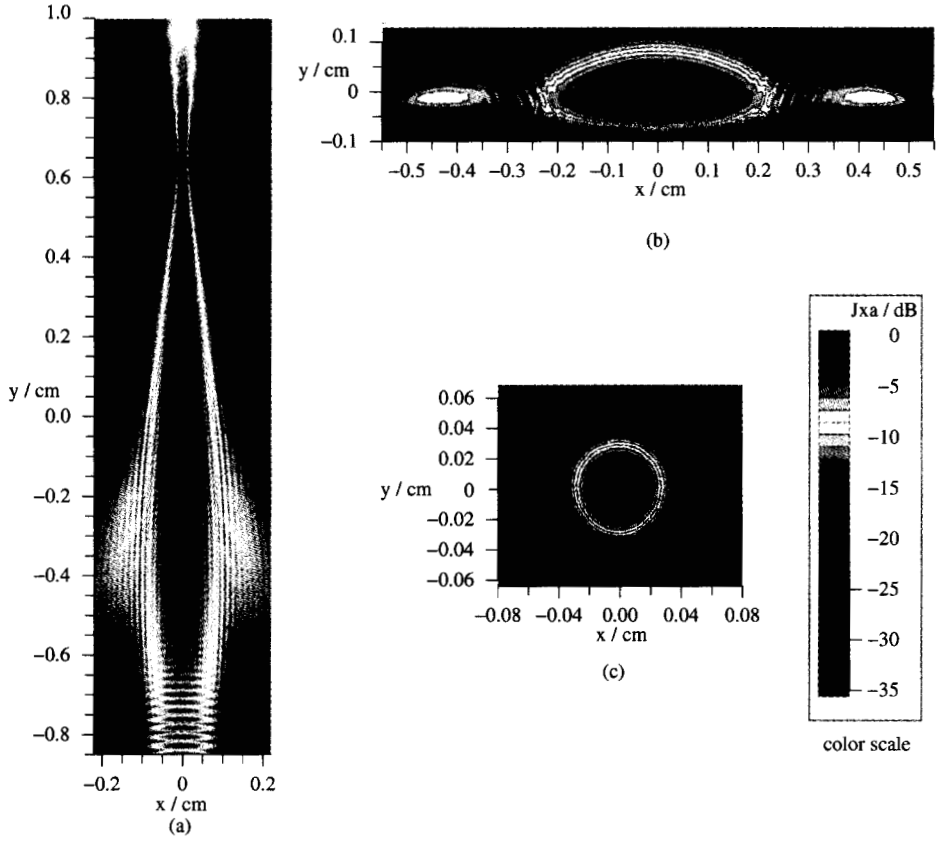

Figure 4. Contours of projected surface current J_x (for x-polarized feed) on the three reflectors: (a) primary, (b) secondary and (c) tertiary. Each panel has 1:1 aspect ratio but scales differ between panels as shown by the attached axes. The common color scale indicates the ratio in dB of J_x to its peak value on each reflector. y is parallel to the toric axis and $x = y = 0$ is the chief ray intercept on each reflector.

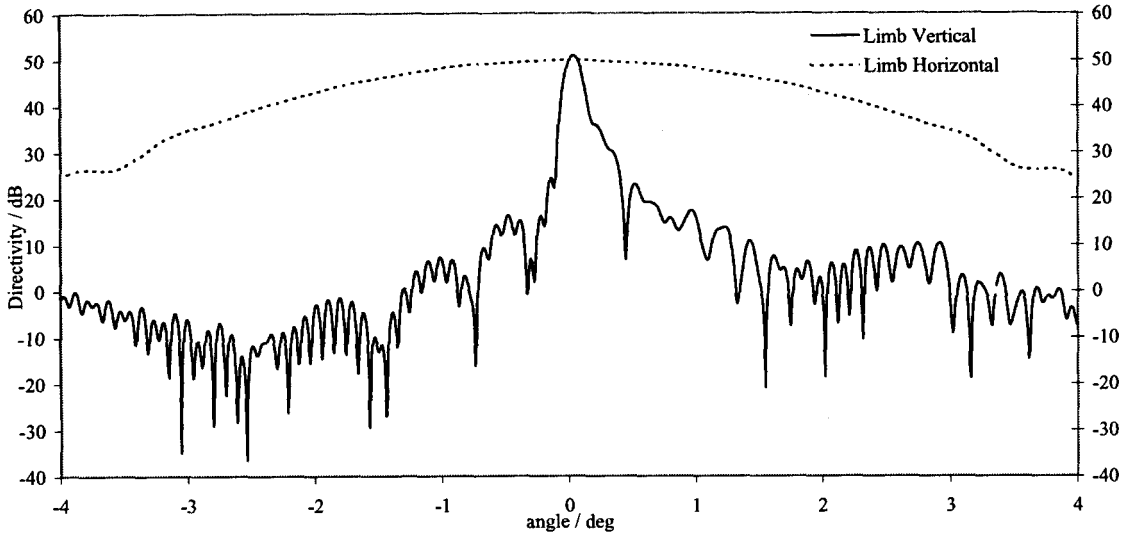

Figure 5. AMLS principal plane patterns calculated using the physical optics model.

5. CONCLUSIONS

The design procedure and resulting configuration of the AMLS antenna have been validated by several independent optical models, and we are confident that a extremely astigmatic system, with reflectors in both the near field and far field according to the principal planes, can give the desired pancake beam at Earth's limb. The progression from paraxial through geometrical and Gaussian beam optics to scalar and vector physical optics models is smooth, so that we are free to choose at which levels we perform optimizations and perturbations. The toroidal reflector concept for the AMLS antenna can provide significant enhancements to limb sounding of the lower stratosphere and upper troposphere in the sub-mm and far IR regimes.

ACKNOWLEDGMENTS

We gratefully acknowledge contributions by many colleagues, especially: Dr. R. Haas for consultation regarding scalar feed horn arrays and lenses; Drs. A. and M. Meinel for review of the optical FOV concept; Ms. V. Ford and Mr. J. Lam for structural design and spacecraft interfaces; Dr. S. Weinreb for MMIC receiver feed array technology and for supporting the physical optics model; Mr. F. Villegas for implementation of the physical optics model and analysis. This work was performed by the Jet Propulsion Laboratory, California Institute of Technology, under contract with the National Aeronautics and Space Administration.

REFERENCES

1. J. W. Waters *et al.*, "The Upper Atmosphere Research Satellite and Earth Observing System Microwave Limb Sounder Experiments," *Journal of the Atmospheric Sciences* **56**, pp. 194–218, January 1999.
2. J. W. Waters *et al.*, "The shuttle imaging microwave system experiment," in *IEEE 1975 National Telecommunications Conference*, **II**, pp. 37–21–37–26, 1975. (Catalog No. 75CH 1015-7 CSC8).
3. R. E. Cofield, "Field of View Calibration of the Microwave Limb Sounder on the Upper Atmosphere Research Satellite," in *International Geoscience and Remote Sensing Symposium*, August 1994.
4. F. T. Barath *et al.*, "The Upper Atmosphere Research Satellite Microwave Limb Sounder Instrument," *Journal of Geophysical Research* **98**, pp. 10,751–10,762, June 1993.
5. R. F. Jarnot *et al.*, "Calibration of the Microwave Limb Sounder on the Upper Atmosphere Research Satellite," *Journal of Geophysical Research* **101**, pp. 9957–9982, April 1996.